JOURNAL OF OPTOELECTRONICS AND ADVANCED MATERIALS Vol. 12, No. 2, February 2010, p. 347 - 353

Nanostructured gold layers. I. Deposition by Vacuum evaporation at small angles of incidence

T. BEICA, S. FRUNZA, I. ZGURA, L. FRUNZA*, C. COTARLAN, C. NEGRILA, A. M. VLAICU, C. N. ZAHARIA[a]
National Institute of Materials Physics, PO Box Mg-07, 077125 Magurele, Romania
[a]*Virology Institute Stefan S. Nicolau of Romanian Academy, PO Box 77-201, 030304 Bucharest, Romania*

Gold layers were deposited at oblique incidence onto glass plates. A B30.2 Hochvakuum Bedampfungsanlage equipment was used in this aim. The deposition conditions were chosen in order to obtain nanostructured layers. Correlations were found among these conditions and the corresponding nomograms were then obtained. Examples of such depositions were given and the layers structure was characterized and additionally supported by observing the molecular alignment given in the liquid crystal cells obtained with these gold layers.

(Received September 15, 2009; accepted February 18, 2010)

Keywords: Nanostructured layers, Gold layers, Vapor deposition, Small incidence angle

1. Introduction

It is already known that self-assembled monolayers (SAMs) can be formed from alkanethiols on the surface of gold, single crystals or films [1-4]; that is why the system has become a tool to study the phenomena on surfaces and to design sensors with targeted applications [5-15]. Thus, several studies have exploited the delicate balance of intermolecular forces underlying the anchoring of thermotropic liquid crystals on surfaces to amplify other molecular interactions, including the presence of proteins specifically bound to functionalized surfaces of gold [16-19]. The structure of SAMs formed on gold from solutions of alkanethiols with more than 9 carbon atoms in the alkyl tail has been extensively studied. A simple geometric calculation [20] indicates a tilt angle of 30° from the surface normal. Grazing-angle infrared spectroscopy in conjunction with ellipsometric measurements [2,3] has confirmed that the alkyl chains are tilted by 30° from the surface normal and rotated around the chain axis by an angle (twist angle) of 52° on surfaces of evaporated gold and Au(111) single crystals.

To achieve columnar structure of gold layer, gold has been vaporized at small angle on the plate surface, meaning large angle with normal direction [21].

This paper reports the experimental conditions for vacuum gold deposition as an improvement of the technique of vacuum deposition of dielectric layer (e.g. SiOx) on glass plates at oblique incidence [22-29] using an equipment Hochvakuum-Bedampfungsanlage B30.2 (Dresden, Germany). In addition the paper develops nomograms (namely two-dimensional diagrams designed to allow the approximate graphical computation of a function) for this installation. Such graphs are used mostly in applications where an approximate answer is appropriate and useful or where to check certain calculated value (see some recent examples of nomogram applications in ref. [30-33]). Then obtaining nanostructured gold layers is illustrated in a few particular cases; some of their features are discussed. The glass plates deposited with nanostructured gold layers were further used to get liquid crystal (LC) cells and the observed alignment of these molecules supports the topography of the substrates.

2. Experimental

2.1. Glass plates

Commercially available float soda-lime glass was cut in plates (32x23x3mm) for vacuum deposition. Their cleaning is an essential step for further works, having a crucial role especially for the adherence of gold layer to the glass plates and for good alignment of liquid crystals in the cells [22]. The method consists in using a cleaning solution followed by its careful removing by ultrasonication, repeated rinse with current and then with deionized water [22].

2.2. Vacuum deposition of gold

Vacuum deposition installation B30.2 is characterized by a manifold deposition room with a diameter of 300mm and a height of 500mm. The vacuum pressure achieved inside was 0.67mPa.

The main device in the deposition room is a carrousel (C1 in Figure 1.a) provided with two sample supports (P1, P2) each carrying 16 small trays for the glass plates. In this device can be simultaneously deposited 16 pairs of glass plates at an incidence angle of ~60º (P1) respectively of ~83º (P2).

Another carrousel (C2 in Figure 1.b) was designed for deposition of frontal layers.

Both carrousels are compatible with the same system of three supports (S in Fig. 1) so that the vaporized material is uniformly deposited by rotating the carrousels around their axis.

The support devices were initially designed for glass

plates with 3mm thickness and dimensions of 70x32mm and respectively 70x23mm, compatible with the trays attachable on the deposition carrousels. For present investigations 32x23x3mm glass plates were used which are compatible with the two tray types. Thus, two plates can be arranged in the tray with 23mm width (down and up positions, Fig. 1.b).

2.3. Methods

To characterize the structure and thickness of the deposited gold layers, several methods were applied among which X-ray photoelectron spectroscopy (XPS), X-ray diffraction (XRD) at grazing angle incidence and reflectometry. XPS studies used a spectrophotometer VG ESCA MkII and software SDP 32, S-PROBE. Grazing angle diffraction was performed with the equipment D8 Advance (Bruker-AXS), in parallel monochromatic configuration: grazing angle was 3º, the measuring domain was 5–65º, the step was chosen of 0.02º. X-ray reflectometry measurements were performed as well under the same conditions.

2.4. Liquid crystal cells

Liquid crystals cells with gold layer on both plates (so called Au-Au type) were further obtained from the deposited glass plates. The two glass plates were thus arranged that the evaporation/deposition direction was anti-parallel (see Fig. 2). The cell thickness was 15μm (by Mylar spacer). The liquid crystal was 4*n*-pentyl-4'-cianobiphenyl (5CB) from Merck, having transition temperature of 35.4ºC. It was introduced in the cell in the isotropic state (at 40ºC).

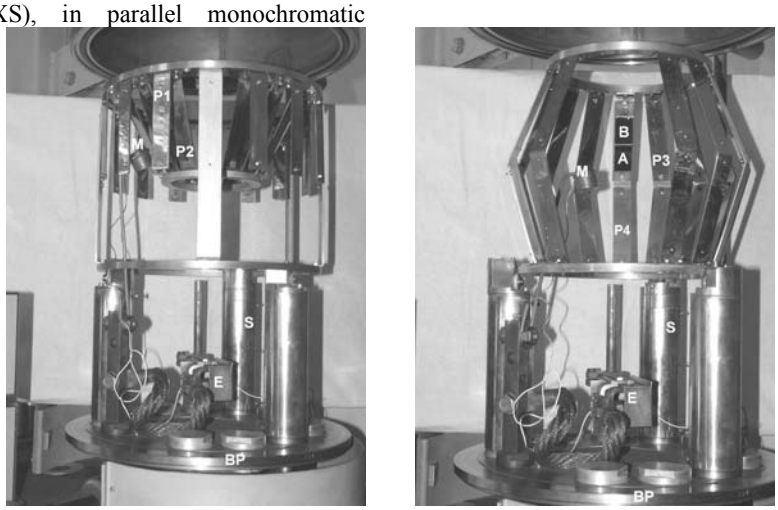

a b

Fig. 1. Carrousels in the B30.2 installation for vacuum deposition: a) C1; b) C2. The component parts are as follows: E – evaporation source (of gold); M – quartz oscillator; P1, P2, P3, P4 – sample supports at preset tilt; S – support for carrousel rotation; BP – base plate. A and B are plate positions on the sample support (down, respectively up).

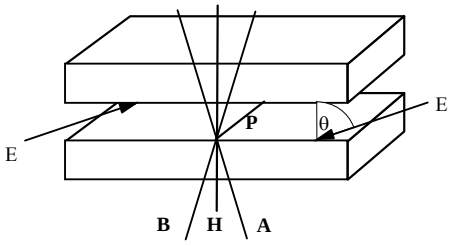

Fig. 2. Assembling two deposited glass plates into a liquid crystal cell. Main evaporation direction E on each plate and possible orientational directions of the LC molecules (A, B, H and P) are shown. E, A, B and H are in the evaporation plane while P is perpendicular onto this plane.

To study the ordering of liquid crystal molecules in these cells direct visualization under crossed polarizers or conoscopic method (under crossed polarizers and convergent light) was applied. The later method used a polarizing microscope (Zeiss Amplival PolU, or Leitz Orthoplan) at which a digital camera (Panasonic DMC-FZ8) was adapted.

3. Results and discussion

3.1. Incidence angles for the installation B30.2

The position of the sample plates and the incidence angles in the installation B30.2 and its carrousels are sketched in Figure 3. We denote by $M(H_M, R_M)$ the midpoints (the limit between A and B plates) on each support considered as reference points; here H_M is the height from base plate (considered as reference level), R_M is the radius from carrousel axis. β is the tilt angle (measured from vertical) for each support. The values of the position and angle parameters in the installation B30.2 are given in Table 1.

Table 1. Parameters of the deposition installation

Sample position	H_M [mm]	R_M [mm]	β [°]	$\theta(L,h_E)$
C1P1	345	135	0	$\pi/2-\alpha(L,h_E)$
C1P2	354	91	27	$\pi/2-\beta+\alpha(L,h_E)$
C2P3	359	108	23	$\pi/2-\beta-\alpha(L,h_E)$
C2P4	250	110	18	$\pi/2+\beta-\alpha(L,h_E)$

3.2. Nomograms to estimate the incidence angles and reduced thickness

Let us make the following notations: h_E is the height of the evaporation source (E) from base plate (BP) and in the following it will be considered as parameter; it takes values in the interval among 30 and 180mm. R and H are the distance from the current point to the carrousel axis and to the base plate respectively. L is the distance from the current point along the plate to the point $\mathrm{M}(H_M,R_M)$ and takes values between –32 and +32mm. The thickness of the deposited layer in actual point on the plate is noted $T(L)$.

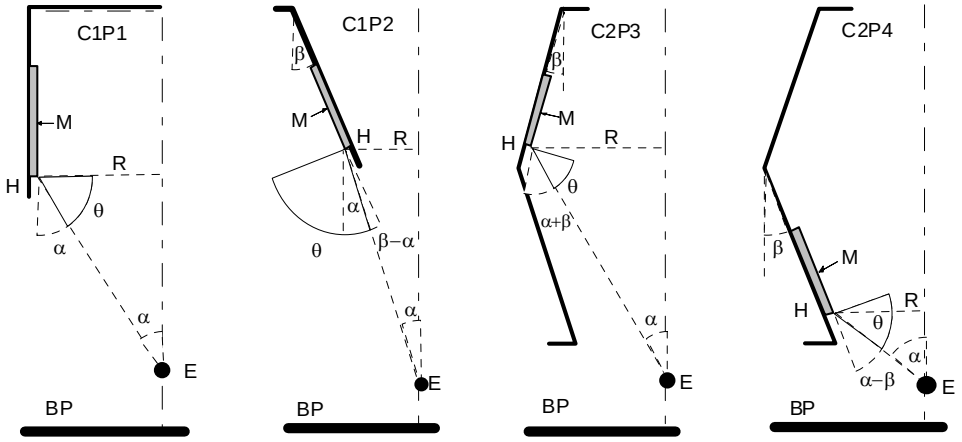

a) b) c) d)

Fig. 3. Position of the plates on the two carrousels and the corresponding incidence angle θ: a) Carrousel C1, position P1 (C1P1); b) Carrousel C1, position P2 (C1P2); c) Carrousel C2, position P3 (C2P3); d) Carrousel C2, position P4 (C2P4). E is the evaporation source, BP is the base plate, M is the midpoint of each support separating the glass plates.

With these notations several dependencies can be established, such as current point height $H(L)$:

$$H(L)=H_M+L\cos\beta \tag{1}$$

current point radius $R(L,h_E)$ for positions P1, P3 and P4

$$R(L,h_E)=R_M+L\sin\beta \tag{2a}$$

or for positions P2

$$R(L,h_E)=R_M-L\sin\beta \tag{2b}$$

Distance d from current point to evaporation source E on the plate can be calculated by simple geometry as

$$d^2(L,h_E)=[R(L,h_E)]^2+[H(L)-h_E]^2 \tag{3}$$

The distances d_{ME} between the reference M points of each device and the vapour source E when the parameter h_E varies is presented in Fig 4.

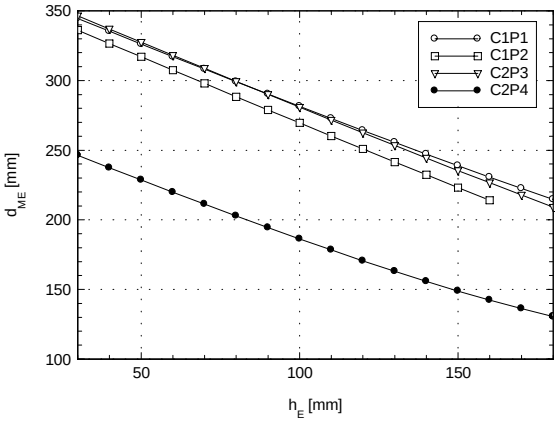

Fig. 4. Distance from the reference point $\mathrm{M}(H_M,R_M)$ and the source E versus h_E.

The angle between the vertical direction and the direction of the emitted vapours, which are arriving at the current point, is

$$\alpha(L,h_E)=\arctan\frac{R(L,h_E)}{\sqrt{[R(L,h_E)]^2+[H(L)-h_E]^2}} \quad (4)$$

The incidence angle $\theta(L,h_E)$ along P1, P2, P3 and P4 plates is further calculated with the above formula, by including $\theta(\alpha,\beta)$ and the values given in Table 1. Because of the geometrical conditions of the deposition there is a variation of the incidence angles $\theta(L,h_E)$ represented as nomograms in the left side of Figure 5. The lowest value of each interval is attained for $h_E=30$mm and the highest value for $h_E=180$mm (with exception of C1P2 where this limit does not exist because $\theta>90°$).

The variation of the thickness layer $T(L)$ along the plates has two sources.

Firstly different points on a considered surface have various distances to the evaporation source. Let consider two elementary surface of unit area, namely the elementary surface $\Sigma(L)$ at the distance d(L) given by eq. 3 and the elementary surface $\Sigma(M)$ placed at the reference point M. Both elementary surfaces have their normal toward the evaporation source E $(\theta=0)$. The thicknesses of the layers simultaneously deposited onto these two elementary surfaces are related each other by the following relationship:

$$T_0(d)=(d_{ME}/d)^2\,T(M) \quad (5)$$

Secondly the variation of the thickness layer along the plates is due to the inclination of the element $\Sigma(L)$ with the angle $\theta(L,h_E)$ so that the layer deposited on it is

$$T(L,h_E)=T_0(d)\cos\theta(L,h_E) \quad (6)$$

To characterize the thickness uniformity on the plates during the same deposition, for a given value of h_E, we define a reduced thickness $T(L)/T(M)$ where $T(M)$ is the thickness in the reference point M, and $T(L)$ is the thickness in the current point L.

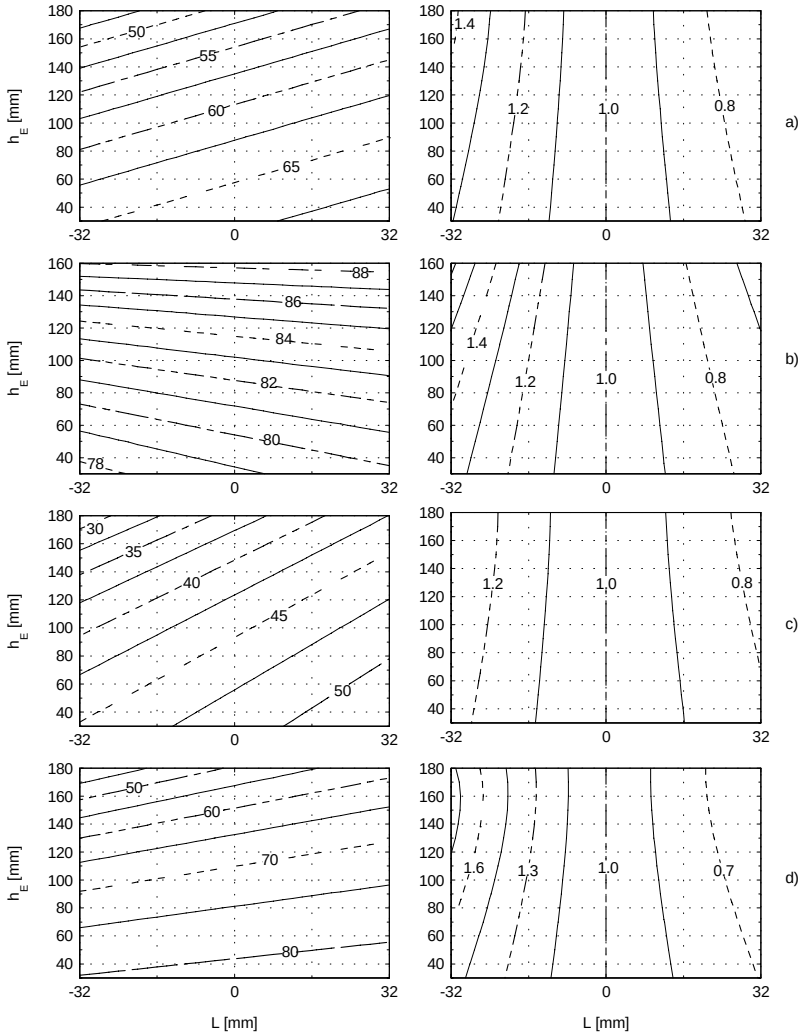

Fig. 5. Nomograms for the incidence angle θ (left part) and reduced thickness T(L)/T(M) (right part) of the possible positions of a sample: a) carrousel C1, position P1; b) carrousel C1, position P2; c) carrousel C2, position P3; d) carrousel C2, position P4.

For the four possible arrangements, the corresponding nomograms allowing the calculation of the incidence angle and reduced thickness are shown in Figures 5a-d. If one uses the devices described above and chooses adequately the source position h_E, it is possible to deposit layers by evaporation at the oblique incidence with an incidence angle θ between 32.5º and 88º. It is possible to obtain the same incidence angle θ using one or more combinations of carrousels and plate positions (Fig. 5). For example the $\theta = 80º$ angle can be obtained using C1P2 (Figure 5b) or C2P4 (Figure 5d), the $\theta = 50º$ angle can be obtained by using C1P1 (Figure 5a), C2P3 (Fig. 5c) or C2P4 (Figure 5d). The uniformity for $\theta(L)$ and $T(L)$ given in nomograms (Figure 5) is the key point for the choice. Another criterion for the parameter choice refers to the quantity of evaporated material used to obtain a desired layer thickness $T(L)$ deposited at a given incidence angle $\theta(L)$. For example in the case of incidence angle $\theta = 80º$ by using C1P2 one requires 1.9 times more gold than C2P4 (the $1/d^2$ dependence must be considered together with values from Fig. 4). However in the last case, C2P4, produces layers with $\theta(L)$ and $T(L)$ less uniform than C1P2.

3.3. Examples of gold layer deposition

Gold deposition was performed at different angles which resulted by the analyzed nomograms. The deposited glass plates were noted $P(m)$ where m is an arbitrary number corresponding to the batch. In Table 2 there are such examples of gold layers deposited at high incidence angle.

Table 2. Gold layers deposited onto glass plates.

Sample	Composition	Incidence angle θ [º]	Thickness [nm]
P(1)	Au/glass	60	20
P(2)	Au/glass	80	~10
P(3)	Au/glass	80	12

XRD investigations at small incidence angles have shown the presence of (micro) crystallyzed gold (see Figure 6). There is a perfect match in position and intensity ratio with the standard files: thus, the peak at $2\theta = 38.23$, is due to Au(111) and that at $2\theta = 44.31$, to Au(200); the small Au(220) peak is visible toward 65 degree. The broad peak at 24.70 belongs to the amorphous glass. Rietveld analysis of these Au(hkl) peaks led to the dimension of the crystallites of 11.5nm. Reflectometry measurements have given the thickness of the gold layer of 22nm (a value which is close to that given by the quartz monitor) and a roughness of 16nm.

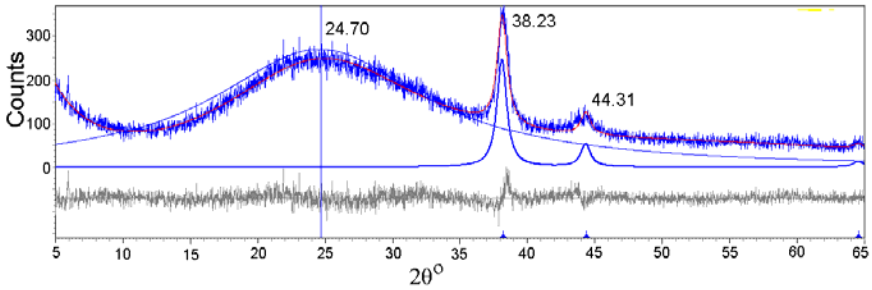

Fig. 6. XRD plot of the sample P (1) and the curves resulted by data smoothing, background fitting and background subtracting. Grey curve is the difference between the experimental and the fitted plot.

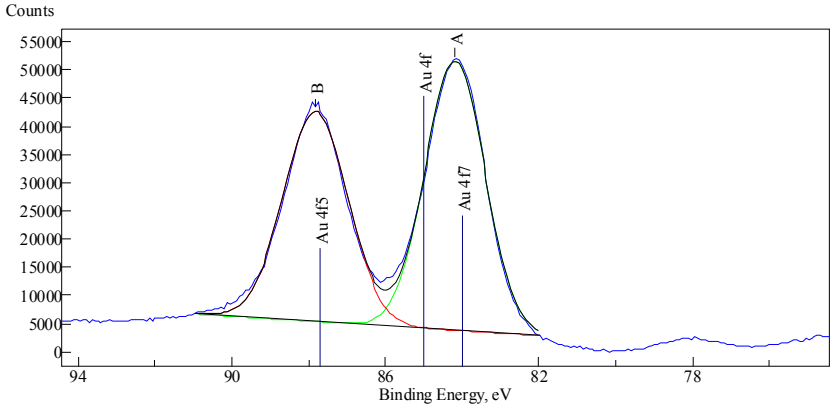

Fig. 7. Main Au 4f lines in the XPS spectrum of the sample P(1). Spectral decomposition of the lines is shown as well, drawn in red and green respectively.

X-ray photoelectron spectroscopy measurements have looked for searching the presence of gold mainly in a metallic state and for testing the impurities (as W, Cu, Fe, Mo) from the carriers (of the evaporation source or of the samples). It was observed in the spectrum (reproduced in Figure 7) that the 4f spin-orbit splitting was measured to be 3.7eV in satisfactory agreement with previous results [34, 35] in the metallic gold. Besides, no impurity appears under the limits of the applied method.

3.4. Orientation of 5CB molecules by the nanostructured gold layers

The orientation of liquid crystal produced by different layers was analyzed by crossed polarizers and in convergent light (conoscopy). For conoscopy measurements the cells have been positioned on the microscope stage like in Figure 2, thus the symmetry axis of the conoscopic interference figure indicates the orienting direction inside the cell while its deviation indicates the tilt against the normal direction to the cell.

The orientation of LC molecules in the cells is always in the plane of gold vapour incidence onto the plate. However, these molecules have a tilt direction and angle which depend on the incidence angle and on the thickness of the gold layer. In Figure 8a the cell with gold layer T_{Gold} = 20nm, $\theta = 60^o$ has a perfect homeotropic orientation (noted H in Figure 2). Depositions at large incidence angle $\theta \sim 80^o$ (and layer thickness $T_{Gold} \sim$ 10nm) have an orientation in incidence plane with a strong tilt type A (Figure 8b) or weak tilt type B (Figure 8c).

In order to use these nanostructured gold layers to LC cells in which the ordering of LC molecules is disturbed due to the presence of certain proteins, many other problems have to be solved among which the adherence of the gold layer to the substrate and the functionalization of gold surface. These problems need more experiments which are in progress and will be described in the next works.

4. Conclusions

There were performed experiments in order to establish the necessary conditions to deposit gold on glass plates at oblique incidence. A B30.2 Hochvakuum Bedampfungsanlage (Dresden, Germany) equipment was used in this aim. Correlations were found among the deposition conditions and the corresponding nomograms were then obtained. These nomograms allowed to estimate the incidence angle and the reduced thickness for other values than those already measured. Several glass plates were deposited with gold layers at different incidence angles; the layers were complex characterized and their structure, discussed.

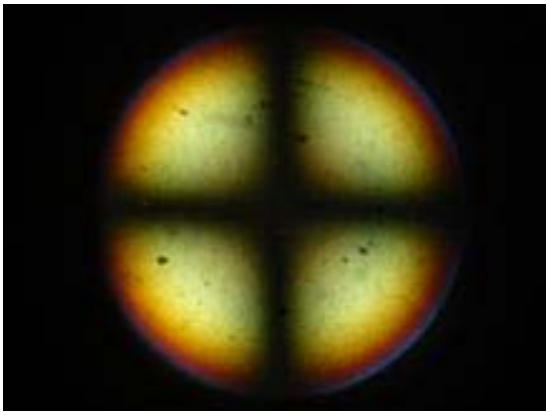

a)

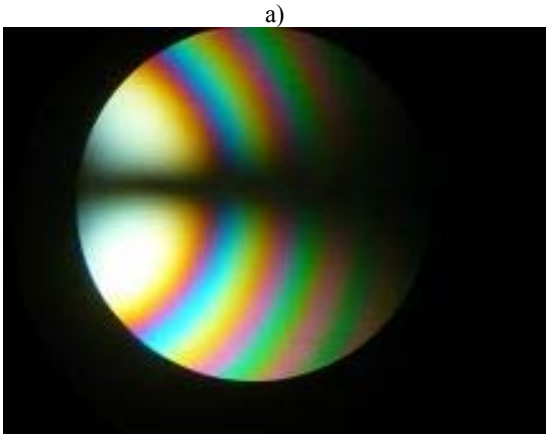

b)

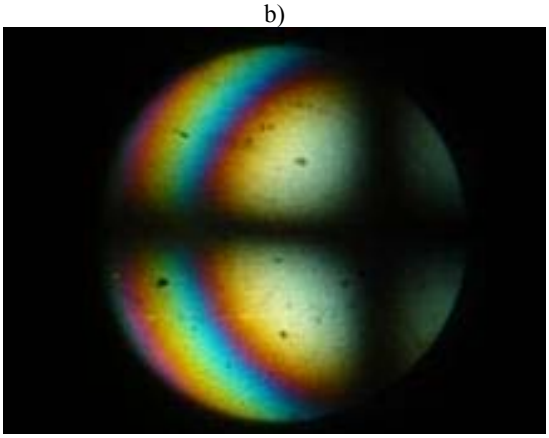

c)

Fig. 8. Conoscopic images of 5CB orientation in the cells each having the two plates deposited as follows: a) P(1); b) P(2); c) P(3).

Acknowledgements

This work was supported by the Romanian Ministry of Education and Research by the PNII Project VIRNANO/2007.

References

[1] R. G. Nuzzo, D. L. Allara, J. Amer. Chem. Soc. **105**, 4481 (1983).
[2] C. D. Bain, E. B. Troughton, Y.-T. Tao, J. Evall, G. M. Whitesides, R. G. Nuzzo, J. Amer. Chem. Soc. **111**, 321 (1989).
[3] M. D. Porter, T. B. Bright, D. L. Allara, C. E. D.Chidsey, J. Amer. Chem. Soc. **109**, 3559 (1987).
[4] G. M. Whitesides, P. E. Laibinis, Langmuir **6**, 87 (1990).
[5] A. Ulman, Chemtech **25**, 22 (1996).
[6] L. H. Dubois, R. G. Nuzzo, Ann. Rev. Phys. Chem. **43**, 437 (1992).
[7] A. Ulman, An Introduction to Ultrathin Organic Films: from Langmuir-Blodgett to Self-Assembly, Academic Press, San Diego, pp 279-298 (1991).
[8] I. Rubinstein, S. Steinberg, Y. Tor, A. Shanzer, J. Sagiv, Nature **332**, 426 (1988).
[9] N. L Abbott, J. P. Folkers, G. M. Whitesides, Science **257**, 1380 (1992).
[10] N. L. Abbott, D. R. Rolison, G. M. Whitesides, Langmuir **10**, 2672 (1994).
[11] R. Drawhorn, N. L. Abbott, J. Phys. Chem. **99**, 16511 (1995).
[12] W. J. Miller, N. L. Abbott, J. D. Paul, M. Prentiss, Appl. Phys. Lett. **69**, 1852 (1996).
[13] V. K. Gupta, W. J. Miller, C. L. Pike, N. L. Abbott, Chem. Mater. **8**, 1366 (1996).
[14] V. K. Gupta, Abbott N.L., Langmuir **12**, 2587 (1996).
[15] V. K. Gupta, Abbott N.L., Science **276**, 1533 (1997).
[16] V. K. Gupta, J. J. Skaife, T. B. Dubrovsky, N. L. Abbott, Science **279**, 2077 (1998).
[17] J. J. Skaife, J. M. Brake, N. L. Abbott, Langmuir **17**, 5448 (2001).
[18] Y.-Y. Luk, M. L. Tingey, D. J. Hall, B. A. Israel, C. J. Murphy, P. J. Bertics, N. L. Abbott, Langmuir **19**, 1671 (2003).
[19] L. A. Tercero Espinoza, K. R. Schumann, Y.-Y. Luk, B. A. Israel, N. L. Abbott, Langmuir **20**, 2375 (2004).
[20] Z. Hou, N. L. Abbott, P. Stroeve, Langmuir **14**, 3287 (1998).
[21] N. L. Abbott, J. J. Scaife, US Patent **6**(288), 392 B1, (2001).
[22] S. Frunza, R. Moldovan, T. Beica, D. Stoenescu, M. Tintaru, Liquid Crystals **14**, 293 (1993).
[23] T. Beica, S. Frunza, M. Giurgea, R. Moldovan, Cryst. Res. Techn. **80**, 875 (1985).
[24] S. Frunza, R. Moldovan, T. Beica, M. Giurgea, D. Stoenescu, Europhys. Lett. **20**, 407 (1992).
[25] S. Frunza, R. Moldovan, T. Beica, L. Georgescu, D. Stoenescu, M. Tintaru, An. Univ. Bucuresti, Fizica **42**, 57-65 (1993).
[26] R. Moldovan, G. Barbero, S. Frunza, T. Beica, Molec. Cryst. Liq. Cryst. **257**, 125 (1994).
[27] R. Moldovan, M. Tintaru, T. Beica, S. Frunza, D. N. Stoenescu, Rom. J. Phys. **42**, 353 (1997).
[28] R. Moldovan, S. Frunza, T. Beica, M., Tintaru V. Ghiordanescu, Cryst. Res. Techn. **32**, 669 (1997).
[29] S. Frunza, G. Grigoriu, A. Grigoriu, C. Luca, L. Frunza, R. Moldovan, D. N. Stoenescu, Cryst. Res. Techn. **32**, 989-997 (1997).
[30] J. S. Booth, D. A. Sangrey, J. K. Fugate, J. Sedim. Res. **55,** 29-36**,**1985).
[31] Yu. Kolomzarov, P. Oleksenko, V. Sorokin, P. Tytarenko, R. Zelinskyy, Semicond. Phys., Quantum Electron. Optoelectron. **6**, 528 (2003).
[32] A. G. Radyuk, A. E. Titlyanov, E. M. Samedov**,** Russ. J. Non-Ferrous Metals **48**, 227 (2007).
[33] B. Reichenbach, I. Solano, P. R. Schwoebel, J. Appl. Phys. **103**, 094912 (2008).
[34] J. Leiro, E. Minni, E. Suoninen, J. Phys. F: Metal Physics **13**, 215 (1983).
[35] N. Aldea, P. Marginean, V. Rednic, S. Pintea, B. Barz, A. Gluhoi, B. E. Nieuwenhuys, X. Yaning, F. Aldea, M. Neumann, Digest J. Nanomater. Biostruct. **1**, 71 (2006).

*Corresponding author: lfrunza@infim.ro